Journal of Alloys and Compounds, 194 (1993) 325–330
JALCOM 7214

Solid state amorphization transformations induced by mechanical alloying

M. X. Quan, K. Y. Wang, T. D. Shen and J. T. Wang
State Key Lab of RSA, Institute of Metal Research, Academia Sinica, Wenhua Road 72, Shenyang 110015 (People's Republic of China)

(Received December 20, 1991; in final form June 5, 1992)

Abstract

The solid state amorphization transformations induced in the Fe–W, (Al or Ni)–(amorphous Fe–Si–B) and Ni–Ti systems were investigated by mechanical alloying. The structure and characteristics of the mechanically alloyed materials were studied by X-ray diffraction, transmission electron microscopy, differential scanning calorimetry, differential thermal analysis, and magnetic measurement. Amorphization by mechanical alloying of the Fe–W system is attributed to a solid state amorphization reaction in which lattice distortion induced by supersaturation of tungsten in the iron crystal and a refinement of grain size may raise the free energy of the iron crystal supersaturated by tungsten above that of the amorphous phase. Amorphization by mechanical alloying of elemental aluminum or nickel metal and amorphous Fe–Si–B alloy can also be obtained within a composition range of the elemental metal. Different amorphization transformation paths are found in the Ni–Ti binary system mechanically alloyed in argon, nitrogen and oxygen atmospheres respectively.

1. Introduction

Over the last few years, a considerable amount of work has been carried out on amorphization induced by mechanical alloying (MA) or mixtures of elemental crystalline powders [1] or by mechanical grinding (MG) of crystalline intermetallic compounds [2]. Amorphization by MA is attributed to a solid state interdiffusion reaction, the kinetics of which is controlled by the excess point and lattice defects generated by plastic deformation. Amorphization by MG is attributed to the accumulation of point and lattice defects which raise the free energy of the faulted intermetallic compound above that of the amorphous phase.

Amorphization by MA is usually obtained in binary alloy systems exhibiting a large negative heat of mixing [3]; this not only provides a thermodynamic driving force for the amorphization reaction but also favors the reaction kinetics by increasing the interdiffusion coefficient [4]. Recently, amorphization reactions have been observed by MA in the Cu–Ag, Cu–Ta, Cu–Cr and Cu–W systems [5–8], all of which exhibit positive heats of mixing. To obtain more insight into the mechanism of MA, we undertook a study of the MA of the Fe–W system, which exhibits a zero heat of mixing in the amorphous state.

Koch *et al.* [9] prepared amorphous $Ni_{60}Nb_{40}$ by MA of the elemental powders in air and helium atmospheres. The crystallization features and the positions of the maxima of the principle peaks in the X-ray diffraction patterns of the system after MA are different in air and in helium atmosphere, owing to the different oxygen concentrations in the alloys. Mizutani and Lee [10] studied the effect of excessive MA on glass formation in an Ni–Zr powder mixture. Partial crystallization takes place which is attributed to oxygen contamination and other impurities. In the present study, we carried out a systematic investigation into the effect of atmosphere on MA.

Weeber and Bakker [11] reported an extension of the glass forming range of the Ni–Zr system by the addition of elemental zirconium to the amorphous Ni–Zr phase through mechanical milling. Recently, Trudeau *et al.* [12] reported ball milling of amorphous $Fe_{78}Si_9B_{13}$ alloy with additional nickel and cobalt powders. When nickel was added, a new amorphous phase containing nickel was obtained, and when cobalt was added, the amorphous phase crystallized completely. The mechanism of the amorphization reaction induced by mechanical milling of elemental metals and amorphous alloys was studied in the present work.

2. Experimental method

For MA of the Fe–W system (Exp.1), elemental powders of iron (99.0 at.%, average size 40 μm) and

0925-8388/93/$6.00

tungsten (99.5 at.%, average size 60 μm) were mixed in equiatomic proportions and used as starting materials.

For MA of the Ni–Ti system (Exp.2), elemental powders of nickel (99.9 at.%, average size 20 μm) and titanium (99.9 at.%, average size 10 μm) were mixed in the composition $Ni_{60}Ti_{40}$ (atomic ratio, same below) and used as starting materials.

For MA of elemental aluminum or nickel metal and amorphous Fe–Si–B alloy (Exp. 3), the following mixtures were used. For aluminum, the relaxed amorphous $Fe_{78}Si_{12}B_{10}$ ribbon was pulverized and mixed with elemental aluminum powder (99.8 at.%, average size 20 μm) to give the composition $Al_{75}(Fe_{0.78}Si_{0.12}B_{0.10})_{25}$. For nickel, the amorphous $Fe_{78}Si_{12}B_{10}$ ribbon was pulverized into a fine powder and then mixed with elemental nickel powders (99.9 at.%, average size 10 μm) to give the following compositions: $Ni_{17}(Fe_{0.78}Si_{0.12}B_{0.10})_{83}$ (sample A), $Ni_{30}(Fe_{0.78}Si_{0.12}B_{0.10})_{70}$ (sample B), and $Ni_{50}(Fe_{0.78}Si_{0.12}B_{0.10})_{50}$ (sample C).

Mechanical alloying was carried out in a conventional planetary ball mill using a hardened steel vial and balls. The rotation rate of the vial was 720 rev min^{-1}. The weight of the as-mixed powder sample for each experiment was about 10 g. The ratios of ball weight to powder weight were 60:1 for Exp. 1, and 30:1 for Exps. 2 and 3. For Exps. 1 and 3, the loaded vials were always sealed under a dry argon atmosphere. For Exp. 2, the loaded vials were sealed under argon, nitrogen and oxygen atmospheres respectively.

After selected times, the milling process was interrupted and a small quantity of milled powder was removed and examined by X-ray diffraction (XRD), transmission electron microscopy (TEM), differential scanning calorimetry (DSC), differential thermal analysis (DTA), and magnetic measurements. For details see refs. 13 and 14.

3. Results and discussion

3.1. Amorphization by MA of the Fe–W system

Figure 1 shows a sequence of XRD patterns for the $Fe_{50}W_{50}$ powder mixture. In the as-mixed state, all of the expected lines of iron and tungsten crystalline elemental powders are observed. From curves (b) and (c), it can be seen that broadening of the Bragg peaks of iron and tungsten and a shift in their positions result in an amorphous halo-like pattern. The changes in the XRD patterns are somewhat similar to those of mechanically alloyed $Ni_{60}Nb_{40}$ [9]. The Bragg peaks related to iron are shifted towards lower angles while those related to tungsten are shifted towards higher angles when compared with the Bragg peaks of pure iron and tungsten. This demonstrates that tungsten atoms are dissolved in the b.c.c. iron crystal while iron atoms are

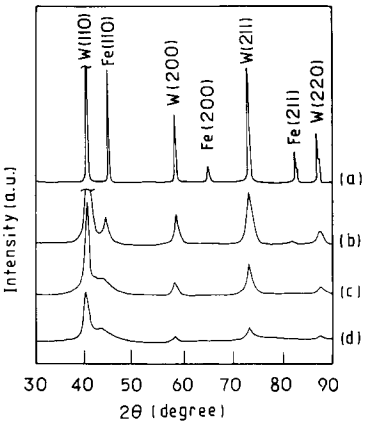

Fig. 1. Comparison of the X-ray diffraction patterns for $Fe_{50}W_{50}$ (a) before milling, (b) after 8 h milling, (c) after 24 h milling, (d) after 84 h milling.

dissolved in the b.c.c. tungsten crystal, causing the lattice parameters of tungsten and iron to change.

The crystallite sizes obtained for the powders milled for 8 h were 4.8 nm for iron and 7.6 nm for tungsten [13]. The lattice parameters were 0.2895 ± 0.0001 nm for iron and 0.3158 ± 0.0001 nm for tungsten after 8 h of milling, as revealed by a Nelson–Riley analysis [15]. The solubilities were determined to be 6.6 at.% tungsten for Fe(W) solid solution and 3.6 at.% iron for W(Fe) solid solution after 8 h of milling [13]. Under equilibrium conditions, iron and tungsten have very limited solubilities (less than or equal to 2.6 at.%) [16]. Thus, it is believed that an $Fe_{93.4}W_{6.6}$ supersaturated solid solution (SSS) and a $W_{96.4}Fe_{3.4}$ SSS are formed after 8 h of milling. Further milling leads to disappearance of the Fe(W) SSS peaks, while the W(Fe) SSS peaks are almost unchanged even after 84 h of milling (see Fig. 1(c) and (d)), indicating that the Fe(W) SSS has transformed into an amorphous phase.

The amorphization reaction during MA has been verified by XRD, DTA, TEM, and magnetic analysis [13]. For a thermodynamic interpretation of amorphization in the mechanically alloyed Fe–W system, the Gibbs free energy diagram was calculated [13], as shown in Fig. 2. The differences in free energy between the crystalline Fe–W SSS and the corresponding amorphous phases $\Delta G^{a-c}(X)$ are approximately equal to 9.5 kJ mol^{-1} for the $Fe_{93.4}W_{6.6}$ alloy and 27.1 kJ mol^{-1} for the $W_{96.4}Fe_{3.6}$ alloy. It can be seen that there is no chemical driving force for the transformation from the crystalline to the amorphous state in the Fe–W system. However, the free energy of a b.c.c. Fe–W solid solution of varying composition $\Delta G^{bcc}(X)$ increases while the difference in free energy between b.c.c. and amorphous Fe–W alloys $\Delta G^{a-c}(X)$ decreases with increasing solubility of tungsten in iron X_w, or iron in tungsten, X_{Fe}. $\Delta G^{a-c}(X)$ has a minimum value of about 7.0 kJ mol^{-1} when $X_w = 30$ at.%, while $\Delta G^{a-c}(X) \leq 7.4$ kJ mol^{-1}

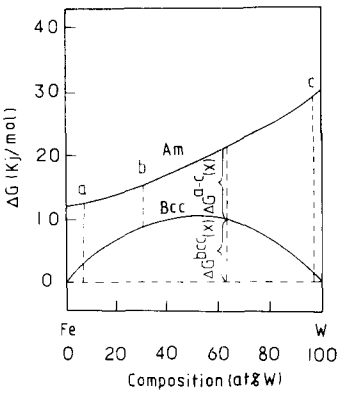

Fig. 2. Gibbs free energy diagram of Fe–W alloys, including the solid solution (b.c.c.) and the amorphous phase (Am). The dashed lines correspond to (a) $Fe_{93.4}W_{6.6}$, (b) $Fe_{70}W_{30}$ and (c) $Fe_{96.4}W_{3.6}$ phases.

when 20 at.% $\leq X_w \leq$ 40 at.%. Therefore, the b.c.c. Fe–W solid solution has elastic energy resulting from distortion of the crystal lattice with the dissolution of iron into tungsten or tungsten into iron.

After MA, the reference state is the ultrafine composite with a large interfacial area. We have taken 4.8 nm as a reasonable grain size of Fe(W) SSS in order to estimate the corresponding stored interfacial energy ΔE_i caused by a refinement in grain size. Accordingly, ΔE_i was estimated to be 9.7 kJ mol^{-1} if the grain morphology of Fe(W) SSS was assumed to be as spherical [13].

In summary, a lattice strain induced by volume mismatch can be obtained with the production of the Fe(W) SSS; the larger the solubility of tungsten in iron, the larger the lattice strain. Furthermore, the mechanically alloyed crystal particles break into fragments and blocks of up to a few nanometers in size, which are misaligned relative to one another. Thus, large lattice distortions arise at the boundaries of the grain or blocks. All of these structural changes result in an increase in the free energy of the Fe–W crystalline phase. The stored energy of the $Fe_{93.4}W_{6.6}$ SSS in the powder mixture milled for 8 h is calculated to be up to 9.7 kJ mol^{-1}, which is comparable with the difference in free energy, 9.5 kJ mol^{-1}, between the $Fe_{93.4}W_{6.6}$ SSS and the corresponding amorphous phase. Thus the increase in free energy due to the refinement in grain size of the nanocrystalline $Fe_{93.4}W_{6.6}$ SSS could provide the driving force for the transition of the material from crystalline to amorphous states by lattice relaxation. The lattice relaxation is verified by the decrease in coercity H_c of powders milled from 8 to 24 h [13].

For W(Fe) SSS, the solubility of iron in tungsten is relatively small (about 3.6 at.% iron) after 8 h of milling. Thus, the lattice strain induced by volume mismatch is also small. The grain size of the W(Fe) SSS in the powder mixture milled for 8 h is about 7.6 nm, which corresponds to an energy increase of about 7.4 kJ mol^{-1}. This energy increase is much lower than the relatively large difference in free energy between the W(Fe) SSS and the corresponding amorphous phase (*e.g.* the difference is about 27.1 kJ mol^{-1} for $W_{96.4}Fe_{3.6}$ alloy). Upon further milling, we found no further dissolution of iron in tungsten or any further decrease in grain size of the W(Fe) SSS. Therefore, the W(Fe) SSS cannot transform into the amorphous state owing to the limited energy increase induced by MA.

3.2. *The influence of atmosphere on MA*

Mechanical alloying is usually performed in an inert atmosphere in order to avoid gas contamination. Since gaseous impurities may be adsorbed in the powder particles and may prevent the solid state interdiffusion reaction during MA, it is important to know how amorphization by MA is influenced by the milling atmosphere. In the present experiment, a planetary ball mill with an additional attachment which allows different atmospheres (argon, nitrogen and oxygen) to be poured into the vial at different milling stages was used. Figure 3 shows the XRD patterns of mechanically alloyed $Ni_{60}Ti_{40}$ in different atmospheres after different milling times [14]. For MA in argon gas, the $Ni_{60}Ti_{40}$ powder mixture could transform directly into the amorphous phase after several hours milling (see Figs. 3(a), (b)

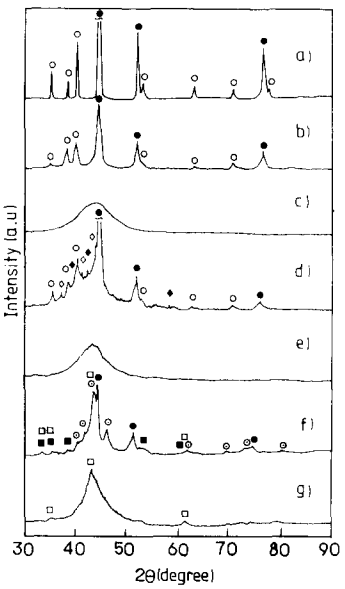

Fig. 3. X-ray diffraction patterns of $Ni_{60}Ti_{40}$ milled in different stages: (a) as-mixed powders, (b) milled for 6 h in argon gas, (c) milled for 20 h in argon gas, (d) milled for 6 h in argon gas and subsequently milled for 2 h in N_2 gas, (e) milled for 6 h in argon gas and subsequently milled for 14 h in N_2 gas, (f) milled for 6 h in argon gas and subsequently milled for 2 h in O_2 gas, (g) after being milled according to process (e) and subsequently milled for 24 h in argon gas; ● nickel, ○ titanium, ◇ Ni_3N, ◆ Ti_2N, ⊙ Ni_3Ti, ■ Ti_2O_3, □ TiO.

and (c)). In the case of MA in nitrogen, the as-mixed powder mixture was first milled in argon gas for 6 h and subsequently milled in nitrogen gas (see Figs. 3(d) and (e)). The results show the existence of nitrides of nickel and titanium. Further milling in nitrogen gas led to complete amorphization of the $Ni_{60}Ti_{40}$ powder mixture.

For MA in oxygen gas, the as-mixed powder mixture was first milled in argon gas for 6 h and subsequently milled in oxygen gas for 2 h (see Fig. 3(f)). The result shows the existence of oxides of titanium and an intermetallic compound of nickel and titanium. Further milling in argon gas up to 32 h (accumulation) led to amorphization of the intermetallic compound, which was attributed to an MG process (see Fig. 3(g)).

The occurrence of the intermetallic compound during MA in oxygen gas was attributed to a self-sustaining reaction [17]. During milling in oxygen gas, grain-refinement by ball milling will proceed through the multiplication and rearrangement of dislocations and also by the rewelding of fractured particles. Oxygen atoms adsorbed on newly created surfaces in the powder particles will be absorbed into the particles by diffusion along dislocations and grain boundaries. Oxygen transport along running dislocations and a vacancy flux into sinks may also contribute to the absorption. Absorbed oxygen atoms will react with the unreacted titanium powder particles. Release of heat due to the oxidation reaction will accelerate the solid state reactions of nickel and titanium into amorphous Ni–Ti in the reaction regions at a temperature less than or equal to 385 °C, and into intermetallic compounds at a higher temperature (above 385 °C) [18]. Compared with the process in which the powder mixtures are milled in argon gas, the solid state reaction during mechanical alloying in oxygen gas can be attributed to a self-sustaining reaction.

3.3. Solid state reaction between crystalline and melt-spun amorphous phases during mechanical milling

To the best of our knowledge, there is no direct evidence that the structures of amorphous phases obtained by melt-spinning or by mechanical alloying or grinding are different. The results of Schwarz *et al.* [19] showed that the structure of $Ni_{40}Ti_{60}$ obtained by melt-spinning and by MA is similar. Therefore, the solid state reaction between crystalline and melt-spun amorphous phases during mechanical milling may be interesting and give some useful information about the solid state amorphization reaction induced by MA and mechanical milling.

Figure 4 shows the XRD pattern of as-mixed aluminum and amorphous $Fe_{78}Si_{12}B_{10}$ powders, which was relaxed below its crystallization temperature, as $Al_{75}(Fe_{0.78}Si_{0.12}B_{0.10})_{25}$ after different milling times [20]. After 16 h of milling, the diffraction peaks of aluminum

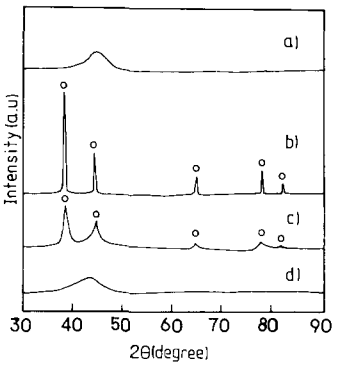

Fig. 4. X-ray diffraction patterns of (a) pulverized relaxed $Fe_{78}Si_{12}B_{10}$ powders, (b) as-mixed powders of $Al_{75}(Fe_{0.78}Si_{0.12}B_{0.10})_{25}$, (c) powder mixture milled for 8 h and (d) milled for 16 h; O aluminum.

almost disappear, but the halo-like peak is much more obvious than that seen after 8 h of milling (see Figs. 4(c) and (d)). For the end-product amorphous sample, the broad diffraction peak of the amorphous phase shifts slightly to lower diffraction angles compared with that of the amorphous $Fe_{78}Si_{12}B_{10}$ phase (see Fig. 4(a) and (d)). The wavenumbers Q_p, related to the maxima of the diffuse peaks in Fig. 4(a) and (d) and defined as $Q_p = 4\pi \sin\theta/\lambda$ ($\lambda = 0.154$ nm), are 30.89 and 30.23 nm^{-1} respectively. The above result indicates that an amorphization reaction was induced by the existent amorphous phase through mechanical milling. The pulverized relaxed powders used in this study were heavily deformed and a high density of defects may be introduced into the amorphous structure. The elastic stress fields associated with the defects may enhance the formation of a metastable phase. Owing to the existing amorphous $Fe_{78}Si_{12}B_{10}$ phase, an Al-based amorphous alloy can be easily obtained by mechanical milling without a nucleation barrier; in other words, the new amorphous phase can be formed easily by growth from the existing amorphous $Fe_{78}Si_{12}B_{10}$ phase. A detailed analysis based on TEM and DSC experiments has proved that a new aluminum-rich amorphous phase is formed by a solid state amorphization reaction between aluminum and the amorphous Fe–Si–B phase during mechanical milling [20].

Figure 5 shows the XRD patterns of mixtures of amorphous $Fe_{78}Si_{12}B_{10}$ powder and elemental nickel powder with various compositions after different milling times [21]. For the powder mixtures with 17 at.% nickel (sample A) and 30 at.% nickel (sample B), new amorphous phases can be obtained by mechanical milling for 24 h (see Fig. 5(a) and (b)). However, for the powder mixture with 50 at.% nickel (sample C), a new amorphous phase and the γ(Fe,Ni) phase can be obtained by mechanical milling for 50 h (see Fig. 5(c)).

The "free volume" model can be used to describe the structure of an amorphous alloy [22, 23]. When

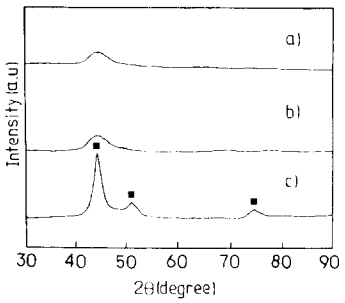

Fig. 5. X-ray diffraction patterns of (a) sample A milled for 24 h, (b) sample B milled for 24 h and (c) sample C milled for 50 h; ■ γ(Fe,Ni).

some nickel atoms diffuse into the amorphous phase under heavy deformation, the "free volume" will play an important role in the short-circuit diffusion paths. It appears that continuous ball milling, *i.e.* fracturing and cold welding, leads to the formation of a large amount of defects. At the same time, the heavy deformation produced during the mechanical milling process accelerates the self-diffusion of nickel and the interdiffusion of nickel in the amorphous phase. The fast anomalous diffusivity of nickel atoms in the amorphous iron-based alloy [24] results in the production of an amorphous alloy which contains nickel. With increasing nickel content in the powder mixture, the metalloid content in the powder mixture decreases. It is difficult to obtain a completely amorphous alloy in a rapidly quenched iron-based metallic glass with a metalloid content less than 12 at.% [25]. In the present case, when the nickel content reaches 50 at.%, the metalloid content becomes less than 12 at.%. Therefore, completely amorphous powder cannot be obtained even after 50 h of milling. During the diffusion of nickel into the amorphous $Fe_{78}Si_{12}B_{10}$ phase, iron atoms from the amorphous phase may enter into the nickel matrix, resulting in the production of the γ(Fe,Ni) phase. In contrast, when the nickel content is relatively low, nickel atoms enter completely into the amorphous matrix. No evidence for the diffusion of atoms from the amorphous matrix into the nickel matrix is observed.

4. Conclusions

(1) A relatively large stored energy can be obtained by the increased solubility of tungsten in iron and by the refinement of the grain size when the Fe–W alloy system is mechanically alloyed starting from pure iron and tungsten powders. Therefore, the free energy of the crystalline Fe(W) SSS is raised above that of the corresponding amorphous phase. This destabilizes the crystalline phase and makes it transform into the amorphous phase.

(2) The amorphization reaction during MA is affected by the milling atmosphere. Argon has no influence on the amorphization process. Nitrogen has a small influence on the amorphization process. However, a small amount of oxygen has a great effect on the amorphization process. An intermetallic compound appeared during the milling of nickel and titanium in an oxygen atmosphere and transformed into an amorphous phase during subsequent milling in argon gas. The formation of the intermetallic compound of nickel and titanium is attributed to the existence of oxygen atoms, resulting in a self-sustaining reaction due to the accumulation of heat release from an oxidation reaction.

(3) Aluminum or nickel atoms can dissolve into the amorphous $Fe_{78}Si_{12}B_{10}$ phase and result in the production of a new amorphous phase containing aluminum or nickel during mechanical milling. The amorphization reaction through mechanical milling may be an interdiffusion process. The defect and strain induced by the milling play an important role in the solid state amorphization reaction of elemental aluminum or nickel metal and amorphous $Fe_{78}Si_{12}B_{10}$ alloy.

Acknowledgment

The work was supported by the National Natural Science Foundation of China (No. 5880014).

References

1 W. L. Johnson, *Prog. Mater. Sci., 30* (1986) 81.
2 R. B. Schwarz and C. C. Koch, *Appl. Phys. Lett., 49* (1986) 146.
3 L. Schultz, *J. Less-Common Met., 145* (1988) 233.
4 L. S. Parken, *Trans. Met. Soc. AIME, 75* (1948) 184.
5 T. G. Richards and G. F. Johari, *Philos. Mag., 58B* (1988) 445.
6 C. H. Lee, M. Mori and U. Mizutani, *J. Non-Cryst. Solids, 117–118* (1990) 733.
7 Y. Ogino, T. Yamasaki, S. Murayama and R. Sakai, *J. Non-Cryst. Solids, 117–118* (1990) 737.
8 E. Gaffet, C. Louison, M. Harmelin and F. Faudot, *Mater. Sci. Eng., A134* (1991) 1380.
9 C. C. Koch, O. B. Cavin, C. G. McKamey and J. O. Scarbrough, *Appl. Phys. Lett., 43* (1983) 1017.
10 U. Mizutani and C. H. Lee, *J. Mater. Sci., 25* (1990) 399.
11 A. W. Weeber and H. Bakker, *J. Phys. F, 18* (1988) 1359.
12 M. L. Trudeau, R. Schultz, D. Dussault and A. Van Neste, *Phys. Rev. Lett., 64* (1990) 99.
13 T. D. Shen, K. Y. Wang, M. X. Quan and J. T. Wang, *J. Appl. Phys., 71* (1992) 1967.
14 K. Y. Wang, T. D. Shen, J. T. Wang and M. X. Quan, *Scripta Metall. Mater., 25* (1991) 2227.
15 J. B. Nelson and D. P. Riley, *Proc. Phys. Soc. London, 57* (1945) 160.
16 O. Kubaschewski, *Iron-Binary Phase Diagrams*, Springer, Berlin, 1982.

17 K. Y. Wang, T. D. Shen, M. X. Quan and J. T. Wang, *Scripta Metall. Mater., 26* (1991) 933.
18 T. D. Shen, M. X. Quan and J. T. Wang, *J. Mater. Sci.,* in press.
19 R. B. Schwartz, P. R. Petrich and C. K. Saw, *J. Non-Cryst. Solids, 76* (1985) 281.
20 K. Y. Wang, A. Q. He, T. D. Shen, M. X. Quan and J. T. Wang, *J. Appl. Phys., 70* (1991) 7158.
21 K. Y. Wang, M. X. Quan and J. T. Wang, submitted to *J. Mater. Sci.*
22 M. H. Cohen and D. Turnbull, *J. Chem. Phys., 31* (1959) 1164.
23 F. Spaepen, *Acta Metall., 25* (1977) 407.
24 B. S. Bokstain, L. M. Klinger, I. M. Razumovski and E. N. Uvarova, *Fiz. Met. Metalloved., 51* (1981) 561.
25 R. Ray, R. Hasegawa, C. P. Chou and L. A. Davis, *Scripta Metall., 11* (1977) 973.